PAPER

Check for updates

Unveiling the corrosion inhibition efficacy and stability of silver nanoparticles synthesized using *Anacardium occidentale* leaf extract for mild steel in a simulated seawater solution

Abdelrahman Osama Ezzat,[a] Victor Sunday Aigbodion, [iD] *[bcd] Hamad A. Al-Lohedan[a] and Chinemerem Jerry Ozoude[e]

Plant extracts used as corrosion inhibitor for mild steel usually degrade as the temperature increases above room temperature. In this study, we used *Anacardium occidentale* (cashew leaf) extract to synthesize silver nanoparticles for improving mild steel's inhibition stability under salinized conditions. Cashew leaves were used as a reducing agent to synthesise silver nanoparticles. The functional group of the silver nanoparticles was determined using Fourier transform infrared spectroscopy. Electrochemical impedance spectroscopy and potentiodynamic polarisation were used to study the corrosion behaviour under simulated seawater by varying the silver nanoparticle concentration between 0.1 and 0.3 g L^{-1}. Scanning electron microscopy and atomic force microscopy were used to obtain information about the surface of the corroded sample. The green silver nanoparticles reduced the corrosion of mild steel up to 90.5% at 40 °C and 90% at 80 °C. At 80 °C, the AgNPs are biochemically and thermally stable, exhibiting a 90% inhibition efficiency. It was established that silver nanoparticles from cashew leaves can be used to improve the stability of mild steel in simulated seawater.

1. Introduction

The use of sustainable materials has gained the attention of researchers around the world today. This is due to the eco-friendly, renewable, biodegradable and non-toxic behavior of the sustainable materials that have been used in various sectors such as energy and power, advanced material development, aviation, drug delivery, tissue engineering, automobiles, defense, and corrosion migration.[1–7] In the area of corrosion migration, the use of sustainable materials such as plant extracts has been a focus of research and development in recent years. This is due to the non-toxic behavior of the plant extracts as compared with the toxic conventional inhibitors for mild steel.[8] Plant extracts such as those from terebinth,[9] watermelon,[10] nettle leaves,[11] tomato pomace,[12] *Piper guineense*,[13] unripe banana peel,[14] cellulose and starch,[15] and the inflorescence of *Musa acuminata*[16] have been used in mild steel anti-corrosion applications in various sectors. However, it was concluded that plant extracts as corrosion inhibitors get slightly degraded with temperature and time, which reduce the plant extract inhibitor efficacy for mild steel at temperatures above room temperature.[8–18] As a result of these limitations, scientists have made an effort to decorate or modify plant extracts to enhance their efficacy when used as corrosion inhibitors above room temperature.

Recent studies have focused on the potential modifications that can be applied to plant extracts to improve their resilience against biodegradation. Extracts have been combined modifications such as sulfate ions,[19] acetylacetonate,[20] zinc salt and zinc oxide,[21] and potassium iodide.[22] These additions improved the effectiveness of plant extracts because of their synergistic effects.[22] However, the use of these reagents is not eco-friendly or sustainable. Recently, researchers have developed silver nanoparticles (AgNPs) using plant extracts as a reducing agent to enhance the corrosion efficacy of plant extracts. Scientists have prepared silver nanoparticles using methods involving *Macrolepiota*,[5] *Garcinia gummi-gutta* leaf,[7] and *Elaeis guineensis*.[23] They all reported improvements in the corrosion inhibition of mild steel.[5,7,23]

The literature above clearly demonstrated the potential of using plant extract-synthesized silver nanoparticles as mild steel corrosion inhibitors. However, despite its recent use in

[a]Surfactants Research Chair, Department of Chemistry, College of Sciences, King Saud University, Riyadh 11451, Saudi Arabia
[b]Faculty of Engineering and the Built Environment, University of Johannesburg, P. O. Box 534, Auckland Park, South Africa. E-mail: victor.aigbodion@unn.edu.ng
[c]Department of Metallurgical and Materials Engineering, University of Nigeria, Nsukka Postal Code, 410001 Nigeria
[d]Africa Centre of Excellence, ACESPED University of Nigeria, Nsukka Postal Code 410001, Nsukka Nigeria
[e]Department: Materials Science and Engineering, University of North Texas, Denton, Texas, USA

various areas, there has been limited research on the use of cashew leaf extract to synthesize AgNPs. For instance, researchers have used the cashew leaf synthesis of AgNPs to enhance the dielectric properties of epoxy composites, enhance the high tension conductivity of Al,[24] and improve the wear behavior and electrical conductivity of Al composites. In this work, we investigate the corrosion prevention by using cashew leaf extract to synthesize AgNPs of mild steel in simulated seawater. Thus, the current work builds upon previous foundation papers. However, more information on the crystalline characteristics, corrosion inhibitory behavior, and adsorption behavior will be covered in this work.

2. Materials and method

2.1 Materials

Table 1 shows the composition of the API 5L pipeline mild steel sample used for the work. The sample was trimmed to 1 cm by 1 cm in size in order to create a functional electrode. In compliance with ASTM D 1141, artificial seawater was used to develop the high-salinity solution.

2.2 Method

2.2.1 Production of the CLE and CLE-AgNPs. The cashew leaf was washed with distilled water and dried. The dried leaves were then ground using a Retsch Planetary Ball Mill PM 400, and the extract (CLE) was then extracted from the ground cashew leaves. A standard procedure was used, which was based on the instructions given in the study by.[24] To make CLE-AgNPs, the cashew leaves were cleaned, and then 100 mL of AgNO$_3$ solution and 100 mL of ethanol were added. The reaction was heated to 100 °C using an electric oven and spun at 2000 revolutions per minute. The heated solution was centrifuged for one hour in compliance with the procedure outlined in the literature to obtain CLE-AgNPs (see Fig. 1).[25,26]

2.2.2 Preparing the API 5L steel. A piece of mild steel (one centimetre by one centimetre) was used as the test material. The samples were subjected to abrasion using metallurgical grit sheets ranging in grade from 120 to 1200, washed with ethanol, and dried with hot air.

2.2.3 Electrochemical analysis. Electrochemical tests using the CHI660D electrochemical equipment determined the corrosion behavior. We conducted the experiment using a standard three-electrode setup. The 1 cm^2 piece of mild steel (the working electrode) and AgCl (the reference electrode) were placed inside a 250 mL beaker of 3.5% NaCl simulated sea water separately with 0.1, 0.2, and 0.3 g L^{-1} CLE and 0.2 g/LCLE-AgNPs. The ranges of CLE and AgNPs used were determined after several experimental trials. The open-circuit potential (OCP) was scanned for 3600 seconds to initiate the electrochemical investigation. The potentiodynamic polarization was determined at −0.5 V to +0.5 V at 0.5 mV s^{-1}. Ranges of 0.1 Hz to 0.5 MHz were used for the EIS corrosion test in the simulated seawater. Eqn (1) and (2) were used to determine the inhibitory efficiency and polarization resistance.

$$\%IE = \frac{(corr.rate)_o - (corr.rate)_i}{(corr.rate)_o} \tag{1}$$

$$R_P = \frac{\beta_a \beta_c}{2.3 i_{corr}(\beta_a + \beta_c)} \tag{2}$$

where i_{corr} = current density, β_a = anodic constant, β_c = cathodic constant, $(corr.rate)_o$ = control sample, and $(corr.rate)_i$ = inhibited sample.

2.2.4 Characterization of the samples. The transmission electron microscopy model JEM-2100F was used to determine the structure and sizes of the CLE-AgNPs. The functional groups of the CLE and CLE-AgNPs were determined using FTIR spectroscopy. The wavelengths of absorption in the range of 400–800 nm were used to determine the UV-visible spectroscopy of the CLE and CLE-AgNPs. The corroded surface was examined with the scanning electron microscope model: VEGA 3 TESCAN.

3. Results and discussion

3.1 TEM image of the CLE-AgNPs

The TEM examination revealed the size and structure of the CLE-AgNPs, as depicted in Fig. 2. The particles, clearly spherical in shape and randomly distributed with 45 to 65 nm particle sizes, demonstrate that the AgNPs can enhance the inhibition efficacy of the plant extract by producing a passive layer to cover the steel surface, aligning with the findings of ref. 3 and 4. The EDS shows high Ag peaks, indicating that the CLE was effective as a reducing agent in the production of CLE-AgNPs. This is consistent with the work of ref. 24–26.

3.2 X-ray diffraction (XRD), UV-Vis spectra and FTIR analysis of CLE and CLE-AgNPs

XRD patterns of the CLE and CLE-AgNPs are displayed in Fig. 3a and b. It is evident that the spectra of CLE-AgNPs exhibit four peaks, whereas the plant extract CLE exhibits reduced diffraction angles and identifiable peaks. The diffraction spectrum seen in the CLE may be explained by the matrix's amorphous nature, which leads to glass diffraction, and the lack of metallic crystal. On the other hand, the CLE-AgNPs spectra showed peaks at $2\theta = 38.01°$, $45.82°$, $64.38°$, and $77.45°$. The findings verify that these peaks line up with the face center cubic (FCC) structure's 311 ($2\theta = 30.5°$), 111 ($2\theta = 38.11°$), 220 ($2\theta = 42.52°$), and 200 ($2\theta = 63.58°$) planes. All of the peaks are sharp and do not expand, indicating that the NPs' crystal structure is free of flaws.

Table 1 Mild steel API 5L pipeline composition

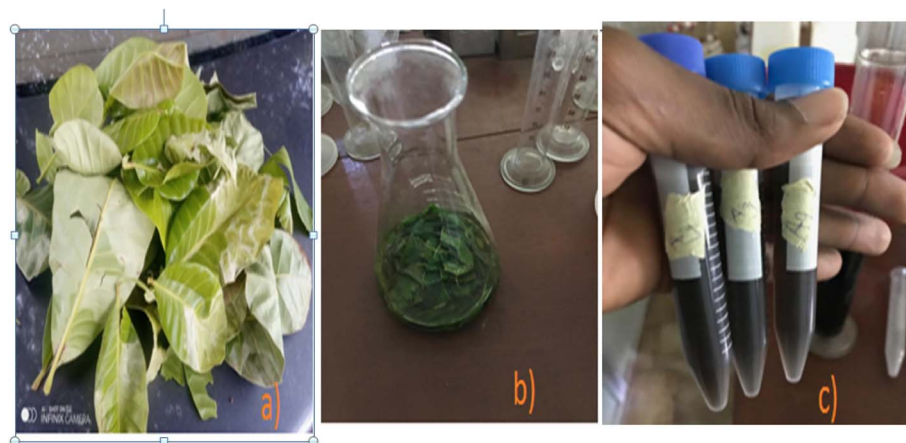| Element	C	Mn	Si	P	S	Cr	Mo	Ni	Ti	Fe
Amount (wt%)	0.12	2.19	0.207	0.280	0.075	0.120	0.0055	0.0066	0.074	Bal.

Fig. 1 Photograph of (a) leaves of cashew (b) mixture of $AgNO_3$ + leaves of cashew (c) CLE-AgNPs.

Fig. 3c displays the UV-Vis spectrum of CLE and CLE-AgNPs. Despite taking the solution's spectrum at 10 minute intervals, Fig. 3c only displays the beginning and final spectra. The plasmon resonance absorption band made by CLE-AgNPs had a different wavelength and absorbance value than the band made by the pure CLE extract. The CLE absorption occurred at $\rho max = 515$ nm, while the CLE-AgNPs absorption occurred at $\rho max = 455$ nm after the full Ag^+ ion bio-reduction reduction. The CLE-AgNPs' absorbance values did not vary across the large absorption range. Most of the plant extract-produced silver nanoparticles in the literature display plasmon absorption in the 400–500 nm region, aligning with the typical Ag plasmon.[27] This finding makes it easier to synthesize AgNPs,[26] and increases the CLE-AgNPs' absorption capacity on mild steel compared to using the CLE alone.

The CLE-AgNPs' FTIR spectra resembled that of CLE (Fig. 3d). Significant peaks were seen in the extracts at 3800, 2500, 1500, and 1100 cm^{-1}. On the other hand, these absorption peaks for the CLE-AgNPs were more intense at 3800 and 1500 cm^{-1}. The Ag^+ in the extract, which displays more intense

FTIR peaks at this point, may enhance the adsorption ability of the CLE-AgNPs. Researchers attributed the 2500 cm^{-1} peak to either the stretching of C–CH$_3$ or C–CH$_2$ vibrations.[29] The 3800 cm^{-1} peak may indicate –N–H stretching vibrations or intermolecular hydrogen-bound –OH stretching vibrations. In the CLE-AgNPs' spectra, the stretching of the H–N vibrations often produces a single, sharp, strong peak at 3800 cm^{-1}, while the stretching of the C=C of the unsaturated ketones N–H amine leads to the absorption peak at 1500 cm^{-1}. The 1100 cm^{-1} feature was associated with CH=CH–, and had good interaction with silver ions. This raises the plant extract's temperature and increases its absorption capacity. The functional groups that cap AgNPs provide the CLE-AgNPs' surface with electron-rich sites and higher adsorption compared to the CLE.

3.3 Open circuit potential (OCP)

Fig. 4 displays the OCP results; it was evident that the inhibited surface shifted the potential to higher positive values as
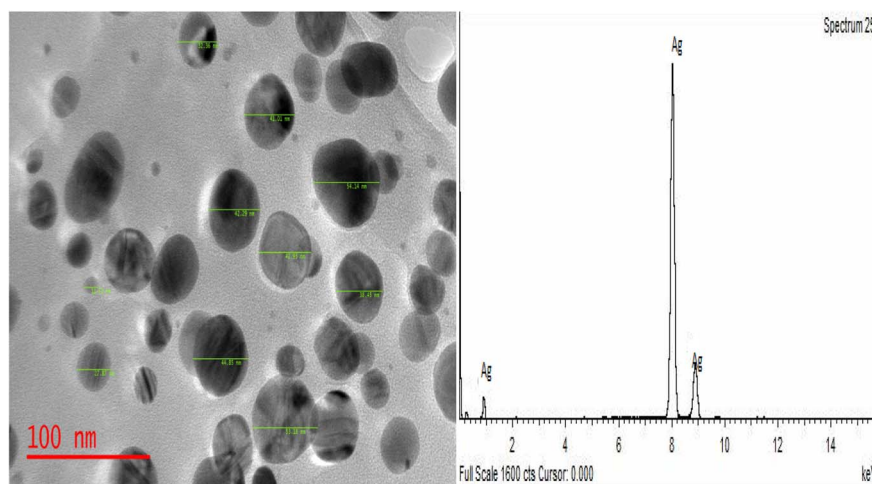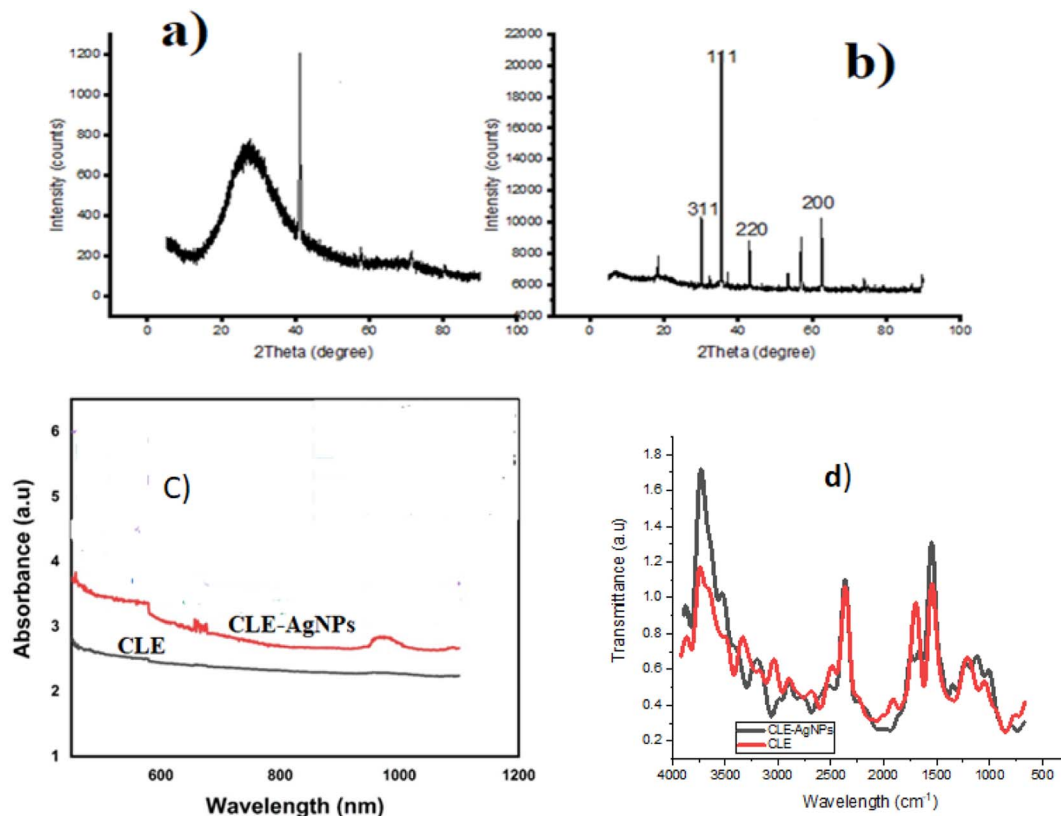

Fig. 2 TEM/EDS of the CLE-AgNPs.

Fig. 3 XRD spectra of (a) CLE and (b) CLE-AgNPs. (c) UV-Vis spectra of CLE and CLE-AgNPs. (d) FTIR analysis of CLE and CLE-AgNPs.
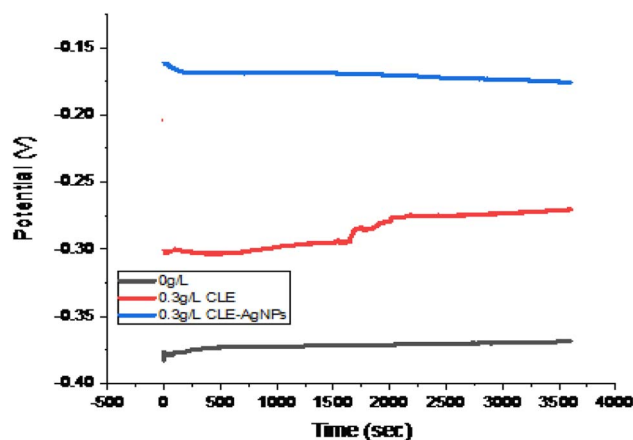

Fig. 4 Variation of the potential with time.

compared with the sample without inhibition over 3600 s. These findings suggest that the inhibitors influence other cathodic corrosion processes, as well as hydrogen development. The UV and FTIR results above demonstrate that the CLE-AgNPs exhibit a higher potential than the CLE due to their higher adsorption ability. Nonetheless, the entire sample exhibits a steady state potential throughout the OCP duration. This is consistent with the work of ref. 30.

3.4 Potentiodynamic polarisation

Fig. 5 displays the samples' Tafel plots. Table 2 displays the electrochemical parameters obtained from the polarization curve analysis. It was evident that the mild corrosion resistance increased as the inhibition concentration increased from 0 to 0.3 g L^{-1}. The values for the corrosion potential (E_{corr}) and current density (I_{corr}) were obtained by fitting curves in the Echem Analyst programme. Changes were observed in both anodic and cathodic E_{corr} values, indicating that the inhibitor may work as a mixed-type.[28] Specifically, an increase in extract content causes a drop in I_{corr}, which in turn causes the corrosion rate to decrease. The present study's findings are consistent with earlier research, which showed that an increase in the amount of inhibitor decreased the I_{corr} and increased the polarisation resistance.[31] The heteroatoms in the extract, adsorbing onto the mild steel surface and reducing the contact between the mild steel and the corrosion medium, were responsible for the decrease in the corrosion rate.[32]

Table 2's inhibition efficiency results revealed that 0.3 g L^{-1} produced a higher inhibitory effectiveness of 83.2% and 94.3% for CLE and CLE-AgNPs, respectively. The inhibitor simultaneously decreases iron dissolution and slows down hydrogen formation. Research demonstrates that the extract blocks the available reaction sites by adhering to the mild steel's surface in the anodic region of the Tafel curve. As the extract concentration rises from 0 to 0.3 g L^{-1}, the surface coverage increases, reducing the corrosion rate and current density. This
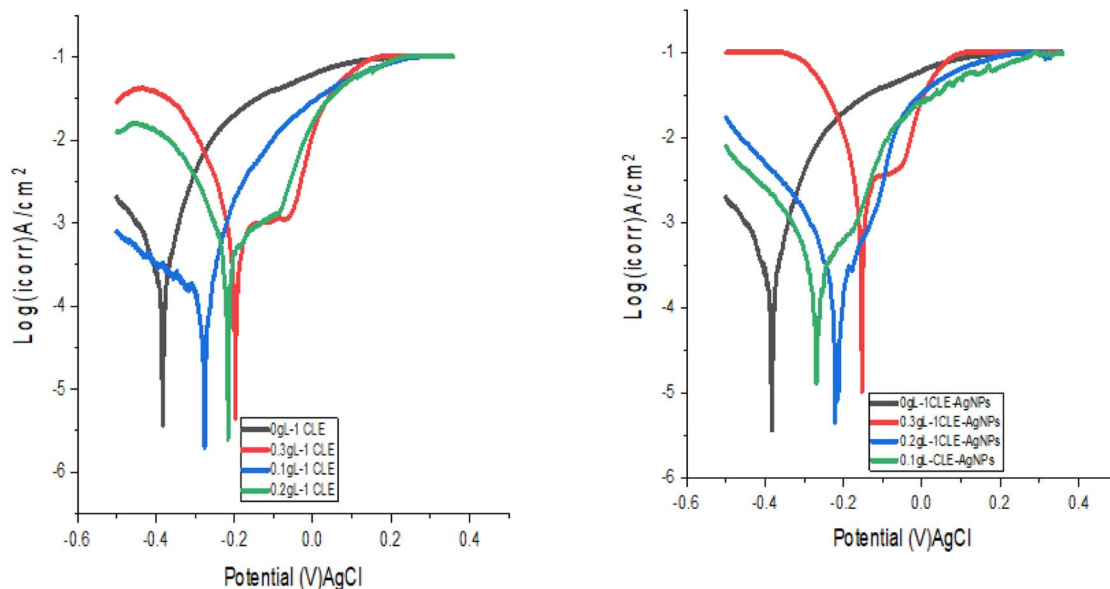
Fig. 5 Variation of the current density with the potential.

demonstrates how a barrier layer covered the surface of the mild steel. The formation of passive films, which separate the mild steel from the corrosion medium, produce a protective coating. This delays the dissolution of metallic ions, which was attributed to the higher inhibition efficiency of CLE-AgNPs.

It has been observed that there are small changes in the values of the Tafel slopes of β_c and β_a, suggesting that the extract functions as mixed inhibitors. While the reaction mechanism stays the same, the cathodic hydrogen evolution and anodic iron dissolution processes diminishes. It was clear that the anodic branch slopes and related anodic Tafel constant (β_c) values for all nanoparticle solutions were very different from the cathodic branch and constant (β_a) slopes. This shows that the AgNPs have a strong influence or effect. Additionally, we observed a shift in the E_{corr} values towards higher values, thereby reinforcing the Tafel constant trend and demonstrating a significant anodic impact. These findings suggest that the adsorption potential of CLE-AgNPs more significantly affects the anodic reaction than the cathodic reaction. The OCP measurement confirms this trend, indicating that processing the extract into nanoparticles (AgNPs) enhances its anticorrosion behavior. This may be because the CLE-AgNPs extract has a higher adsorption capacity; there are more electron clouds, which allow for the adsorption onto mild steel surfaces. The inhibition efficiency increases with AgNPs content, but remains relatively constant when compared to the plant extract.

3.5 EIS analysis of the samples

Fig. 6a and b shows the Bode phase and Nyquist plots in the corrosive medium for mild steel and in a saline solution. EIS fitting was used to get this data using the circuit model shown in Fig. 6c. The Nyquist curve displays a characteristic depressed semicircle pattern, and the diameter of the semicircle positively correlates with CLE and CLE-AgNPs, in line with previous research.[6,7]

The Bode phase angle also demonstrated that the steel surface and electrolyte only make one contact. One possible

Table 2 Results of the potentiodynamic polarisation

| g L^{-1}	E_{corr} (V)	I_{corr} (A cm^{-2})	β_c	β_a	R_p (Ω cm^2)	C_R (mpy)	Θ	IE%
CLE								
0	−0.412	3.84×10^{-3}	5.810	10.757	8.7	1.150×10^3	0	0
0.1	−0.289	2.13×10^{-3}	5.671	4.938	9.8	5.21×10^2	0.555	55.5
0.2	−0.197	1.319×10^{-3}	5.719	0.971	10	3.75×10^2	0.674	67.4
0.3	−0.165	5.164×10^{-4}	5.559	1.099	31	1.938×10^2	0.832	83.2
CLE-AgNPs								
0	−0.412	3.84×10^{-3}	5.810	10.757	8.7	1.150×10^3	0	0
0.1	−0.143	3.17×10^{-4}	7.261	5.37	92.4	8.58×10^1	0.926	92.6
0.2	−0.135	1.8×10^{-4}	8.932	6.78	129.2	7.901×10^1	0.931	93.1
0.3	−0.103	1.427×10^{-4}	9.458	4.433	143.9	6.582×10^1	0.943	94.3
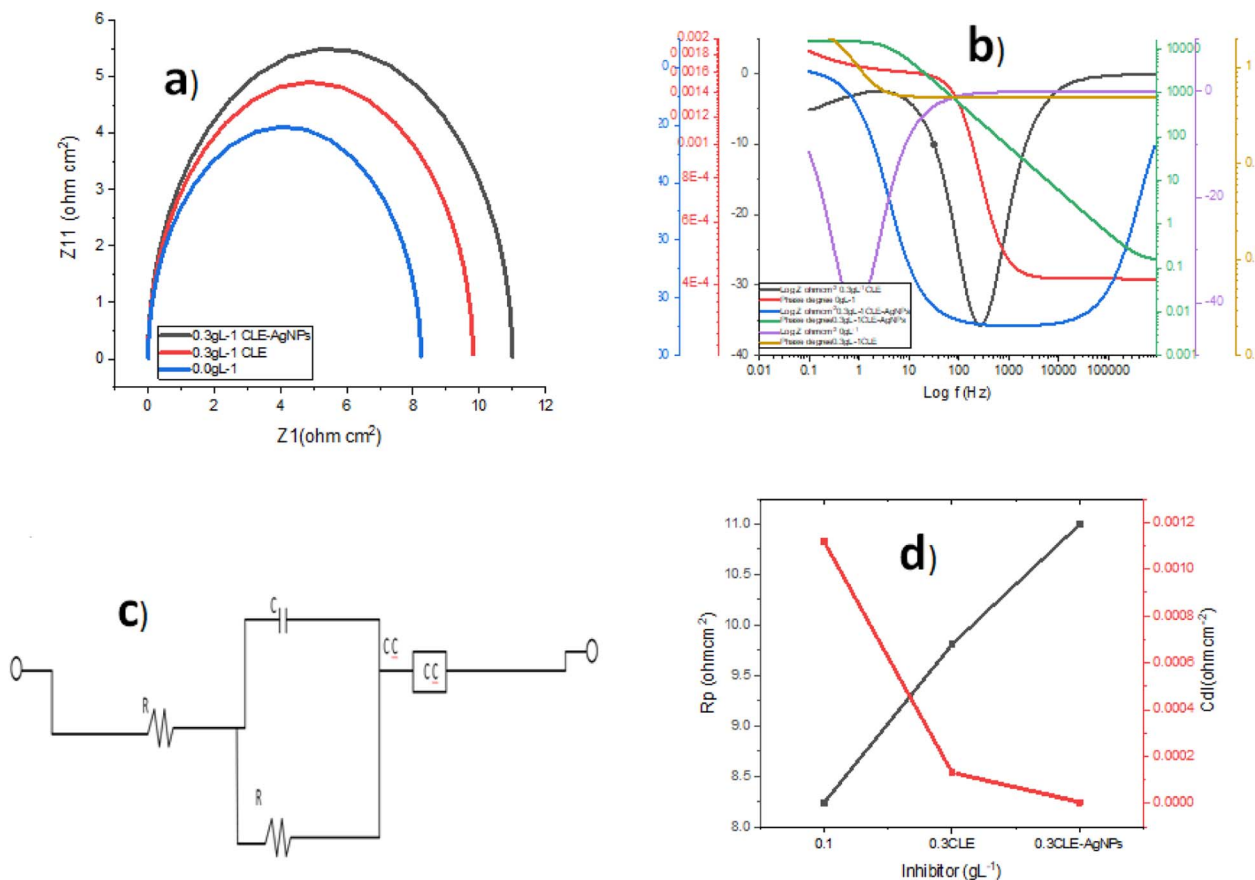
Fig. 6 (a) Nyquist curves and (b) Bode curve of the samples: 0 g L^{-1}, 0.3 g L^{-1} CLE and 0.3 g L^{-1} CLE-AgNPs. (c) EIS fitting circuit model. (d) Plots of polarization resistance (R_p) and capacitance of the interface (C_{dl}) with inhibitor.
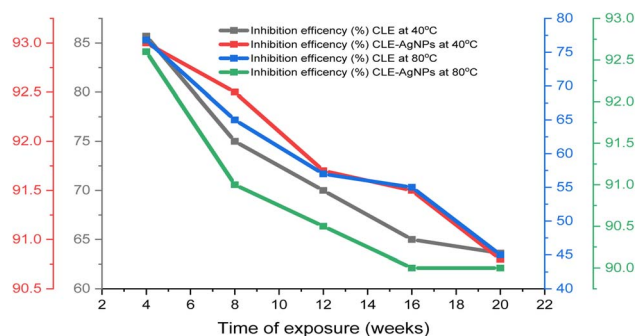

Fig. 7 Inhibition stability of the extracts.

explanation for this result is a protective coating of biomolecules from CLE-AgNPs covering the steel's surface. Inhibitors cause the R_{ct} levels to increase, while the C_{dl} values decrease (Fig. 6d). A decrease in the local dielectric constant and an increase in the protective film are associated with lower C_{dl} values.[30] The higher capacitive loop, as shown by the Nyquist plots, revealed that a protective layer was formed on the mild steel surface. The polarization resistance (R_p) increased in proportion with the inhibitor's type, while the interface capacitance (C_{dl}) decreased for the inhibitor CLE-AgNPs. This was

attributed to the decrease in both electrical double layer's thickness and the local dielectric constant. This suggests that the inhibitor functions at the solution/metal interface by adsorption, and that the reduction in C_{dl} values is caused by water molecules replacing the surface of the electrode and the reduced dissolution of the metal.[30] A CLE-AgNPs sample with a larger semicircle diameter or greater charge transfer persistence is often indicative of a higher corrosion resistance. It is believed that the corrosion products produced at the coating surface are what cause the drop in corrosion rate that is seen when the charge transfer resistance rises.

3.6 CLE and CLE-AgNPs stability

Using weight loss measurements during a 20 week preparation period at 40 and 80 °C temperatures, the stability of the CLE-AgNPs was evaluated using the simulated seawater. Before this, we kept the already-produced samples at room temperature in laboratory cabinets within reagent bottles. The weight loss technique was used to examine the effectiveness of the maximum addition of CLE and CLE-AgNps every four weeks (starting from the date of the first preparation) at the investigated temperatures. The efficiency of CLE began to decrease after eight weeks, according to the results (Fig. 7), whereas the CLE-AgNPs maintained their efficiency the whole time. At 80 °C,
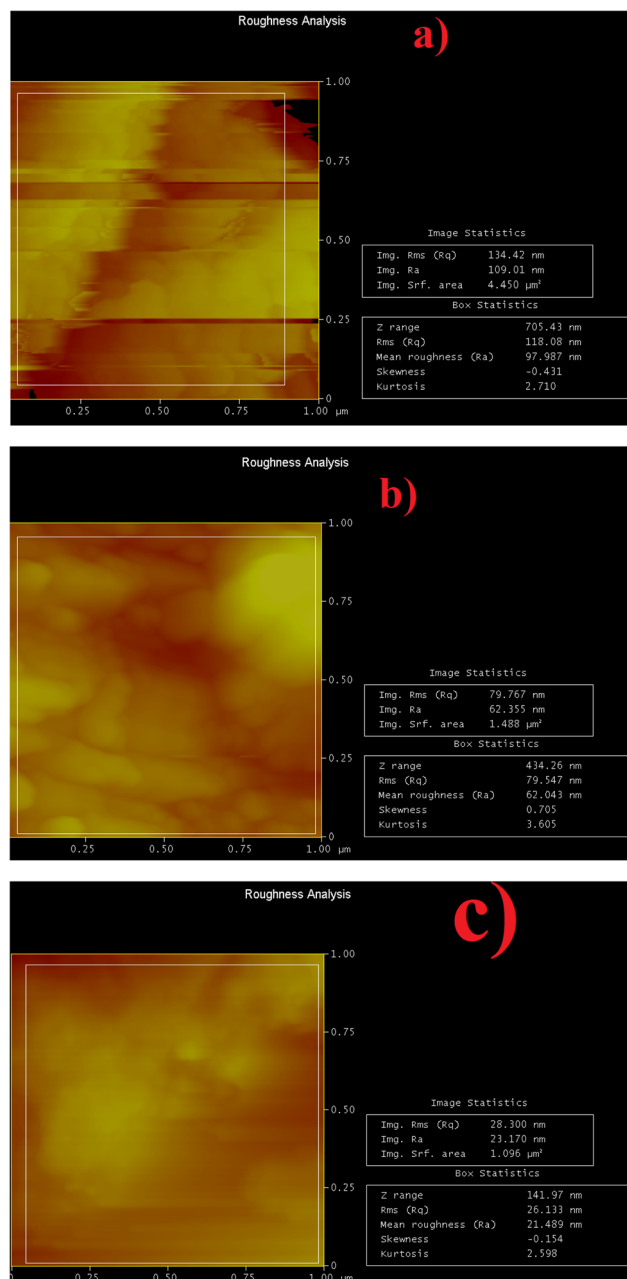
Fig. 8 AFM analysis of the corroded surface: (a) 0 g L^{-1}, (b) 0.3 g L^{-1} CLE, (c) 0.3 g L^{-1} CLE-AgNPs.

the CLE extract's efficiency started to fall more sharply. The relative ease of thermal and biodegradation in the plant extract may help explain this phenomenon. The sample with CLE-AgNPs was more stable during the investigation period because of the biochemical properties of Ag$^+$, which showed low degradation during this time with an inhibition efficiency of 90% at 80 °C.

3.7 Corrosion mechanism

The corrosion mechanism was studied in order to better understand the behavior of the mild steel in the saline environment in the presence of an inhibitor and without an inhibitor. The initiation phase stage was shown by the dissolution of the mild steel, and the breakdown of the passive layer in the anodic region was shown by a chemical reaction.[10–12] However, in the cathodic region, oxygen reactions occurred through the coverage mechanism. Eqn (3)–(5) may be used to represent the whole response in the following manner:

$$Fe = Fe^{2+} + 2e^- \quad (3)$$

$$O_2 + 2H_2O + 4e^- = 4OH^- \quad (4)$$

$$4Fe + O_2 + 2H_2O = 4Fe(OH) \quad (5)$$
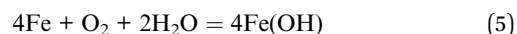
An excessive concentration of positive Fe^{2+} ions occurs in the anodic area as a result of the metal's continuous dissolution. Charge neutrality occurs when the Cl$^-$ ions leave the electrolyte at the same time. The combination of the Fe^{2+} and ion (Cl$^-$) results in the formation of ferric chloride, as shown in eqn (6).

$$Fe^{2+} + Cl^{-1} = FeCl_2 \quad (6)$$
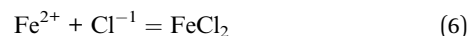
Eqn (7) illustrates how FeCl$_2$ and H$_2$O combine to produce Cl$^-$, H$^+$, and FeOH. The repassivation process occurred as a result of the reaction of Cl$^-$ and H$^+$ ions. A faster anode disintegration leads to a higher rate of FeCl$_2$ generation because it speeds up the chloride ion migration. The extracts slow down the increase in metal degradation. CLE-AgNPs, on the other hand, were more stable and resistant to corrosion than CLE because they had better biochemical properties, less direct contact with mild steel, and higher electronegativity.

$$FeCl + H_2O = FeOH + H^+ + Cl^- \quad (7)$$

3.8 AFM structure of the corroded samples

The surface of the mild steel submerged in NaCl, both with and without CLE-AgNPs, was investigated by AFM. Fig. 8 displays the 2D pictures of the amplitude and topographical surfaces, as well as the 3D photographs of the pits and peaks on the surfaces that we were able to capture. The blank solution displayed a high, rough surface with numerous peaks and pits, indicating significant damage from the rapid corrosion of NaCl. The 0 g L^{-1}, 0.3 g/CLE, and 0.3 g L^{-1} CLE-AgNPs yielded the greatest peak heights (Sp) of 97.98, 62.04, and 21.48 nm above the surface mean plane, respectively, while the deepest pits (Sv) were measured 105.1, 78.9, and 47.8 nm below the surface mean plane. The blank sample exhibited higher peaks and deeper holes due to the NaCl attack.[27] When compared to the blank sample, the CLE-AgNPs reduced pitting by about 54.42% and peak heights by 78.08%, indicating a very effective anticorrosion action. The RMS heights (Sq) measured are as follows: 118.08 nm, 79.55 nm, and 26.13 nm for 0 g L^{-1}, 0.3 g L^{-1} CLE, and 0.3 g L^{-1} CLE-AgNPs, respectively. The addition of CLE-AgNPs caused an average reduction in peak height by corrosion degradation, which was about 77.87% lower than that of the blank.
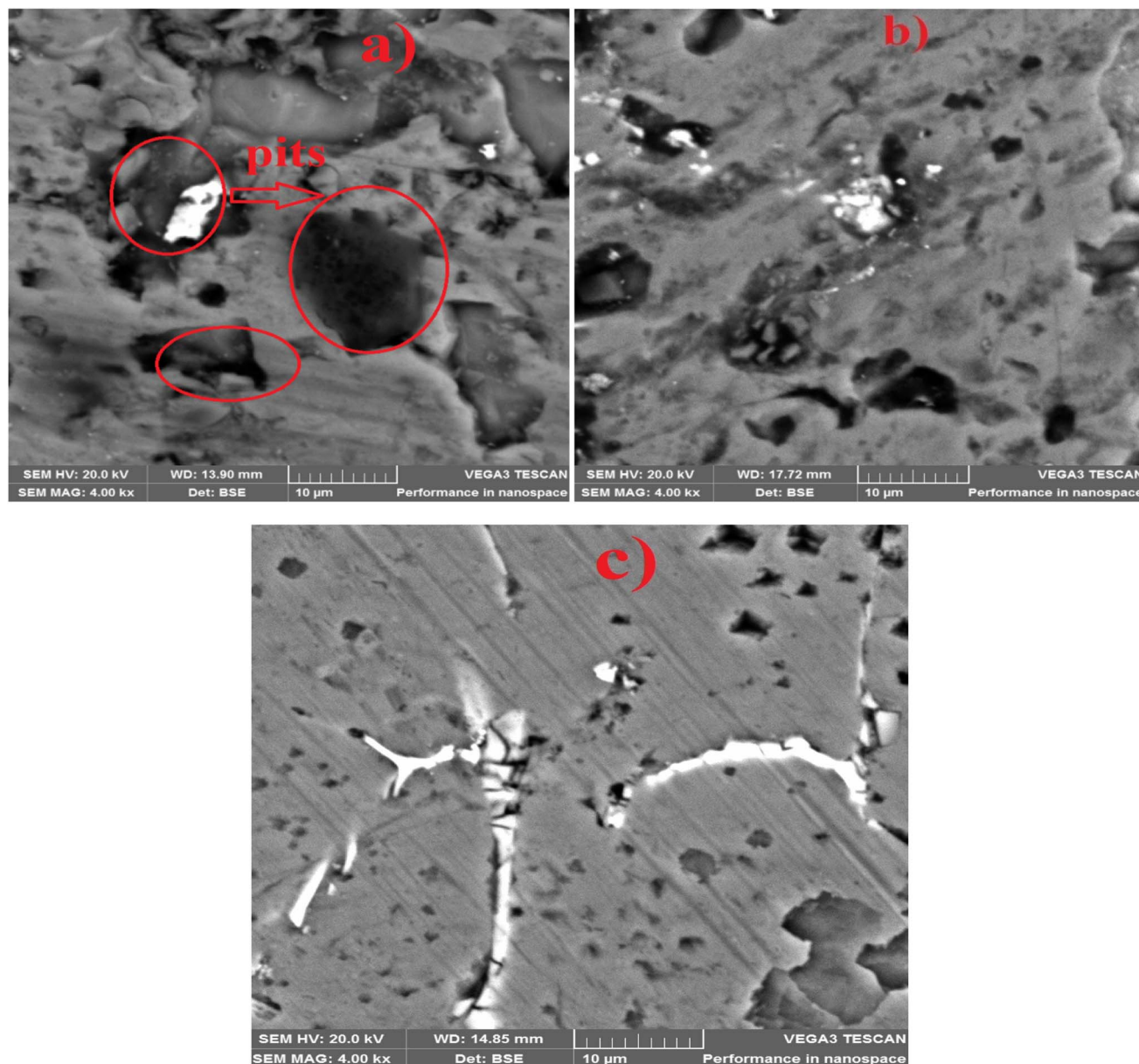
Fig. 9 Corroded surfaces of (a) 0 g L^{-1}, (b) 0.3 g L^{-1} CLE, (c) 0.3 g L^{-1} CLE-AgNPs.
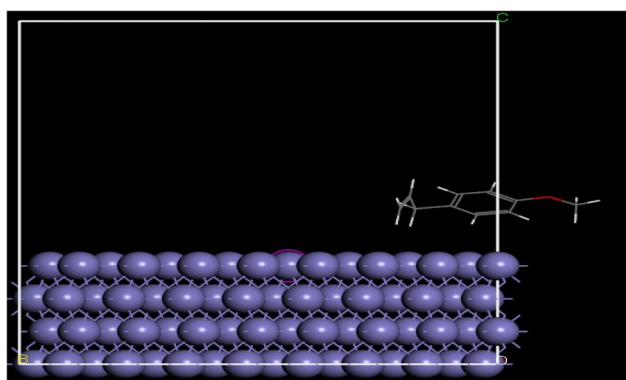

Fig. 10 Simulation structure using MD.

3.9　Corroded surface images by SEM

The SEM surface of the corroded samples, as shown in Fig. 9, shows fewer flaws, pits, and corrosion damages in the 0.3 g L^{-1} CLE-AgNPs sample compared to the other samples under investigation. The sample without an inhibitor showed higher corrosion damages, pits, and uneven holes, indicating mild steel dissolution in the saltwater environment and an increase in the anodic reaction. The CLE-AgNPs extracts' ability to inhibit the corrosion helped delay and slow down the rate at which the mild steel came into contact with the saltwater environment. This study suggests that CLE-AgNPs may efficiently inhibit the corrosion of mild steel under saline condition. This was used to support the AFM results discussed above.

Table 3 The molecular dynamics simulation results

Total energy (kcal mol^{-1})	Energy of adsorption (kcal mol^{-1})	Energy of rigid adsorption (kcal mol^{-1})	Deformation energy (kcal mol^{-1})	dNi/dEad	Energy of binding (kcal mol^{-1})
−56.601	−61.032	−54.200	−15.173	−61.032	−61.032

3.10 Molecular dynamics simulations (MD)

Molecular dynamics simulations (MD), a tried-and-true computational chemistry tool, was used to identify obscure elements that aid in characterizing and understanding the adsorption interaction forces of plant extracts with mild steel. It is believed that the 1100 cm^{-1} feature, which was associated with CH=CH– and had good interaction with silver ions from the FTIR data, was used for the MD at 0.3 g L^{-1} CLE-AgNPs. In Materials Studio, the adsorption finder was used to determine the energy of the Fe molecular adsorbates. Using the Monte Carlo technique, this module exhaustively explores the entire surface interactions and adsorbate configurational space. It considers a number of degrees of freedom, including the adsorbate's surface translations and rotations. Finding and evaluating the combinations with the lowest energy levels is the main goal. Many investigations used this module, which made evaluating the lowest-energy surface-adsorbate configuration (SAC) easier.

To determine the best SAC and the lowest energy configuration, molecular adsorbates were pre-adsorbed. The adsorption calculation had to determine the minimal energy state of the entire system, as shown in Fig. 10. Table 3 displays a number of outputs and descriptors, including the total energy of the adsorbate-substrate surface. The total energy comprises the combined energies of stiff adsorption, energy deformation, and the energies of adsorbed components. The "adsorption energy (kcal mol^{-1})" is the amount of energy needed or released when components stick to a relaxed adsorbate on the substrate. Table 3 includes the adsorbate-substrate energy (in kcal mol^{-1}), expressed as (dEads/dNi). Table 3 displays the interaction energy (E interaction) and binding energy (E binding) values between the Fe (110) surface and CLE-AgNPs, particularly when the systems are in equilibrium. The findings show that the inhibitor being studied has negative interaction energies (−E binding), which means that natural organic substances naturally stick to the surface of the Fe (110). Interestingly, greater energy adsorption values show that some natural organic component compounds are more effective at inhibiting corrosion. Table 3 provides evidence that CLE-AgNPs exhibit a higher −E binding value, suggesting a higher adsorption capacity, in line with the experiment results.

3.11 Comparative analysis

Due to the effects of biochemical agents, many corrosion inhibitors made from plant materials are unstable and quickly deteriorate when exposed to heat or kept for extended periods of time. This limits the use of these specific corrosion inhibitors. Documentation exists for similar applications of a variety of plant-based corrosion inhibitors, including the compounds described in this work. For example, a recent assessment recorded several of these items. In comparison, CLE-AgNPs either matched or outperformed a lot of these corrosion inhibitors. The extracts from *Allium cepa* peels,[27] banana peels (*Musa paradiaca*),[28] orange peel extract,[29] *Solanum macrocarpon* leaves,[30] watermelon peel extracts,[31] and tomato pomace extract[32] are a few examples. Additionally, new research suggests that CLE-AgNPs work better than nanoparticles made from *Musa paradisiaca* peels,[28] *Macrolepiota* leaves,[5] *Solanum macrocarpon* leaves,[30] and *Garcinia gummi-gutta* leaves.[7]

4. Conclusions

In this work, we synthesized green silver nanoparticles using silver nitrate and cashew leaf extract to improve the corrosion inhibition and stability of mild steel in a saline environment. The extract and silver nanoparticles were then analyzed and assessed as an inhibitor of mild steel in a saline environment. The green silver nanoparticles have an FCC structure and plasmon absorption at 455 nm. They are perfectly crystalline, with most of the Ag atoms lined up along the (111) plane. The synthesized eutectic AgNPs have spherical forms, are monodispersed, and have a particle size of 45 nm. The surface of the green silver nanoparticles had more O sites than the pure extract, indicating a stronger adsorptive potential. Inhibitors of mixed dominating influence as anodic half reactions, the green silver nanoparticles work to stop the corrosion of mild steel 90.5% of the time at 40 °C and 90% of the time at 80 °C. The addition of green silver nanoparticles prevents corrosion on the steel surface by reducing the peaks and pits caused by corrosive attack by 78.08% and 54.42%, respectively. At 80 °C, the CLE-AgNPS is biochemically and thermally stable, with a 90% inhibition efficiency. In saline and marine applications, green silver nanoparticles from cashew leaves are a cost-effective, environmentally friendly substitute for corrosion inhibitors.

Data availability

The authors confirm that the data supporting this study's conclusions are included in the publication.

Author contributions

All authors contributed 100 percent to the study's development, from experimentation to analysis.

Conflicts of interest

There is no conflict of interest in this work.

Acknowledgements

References

1 S. R. Al-Mhyawi, Green synthesis of silver nanoparticles and their inhibitory efficacy on corrosion of carbon steel in hydrochloric acid solution, *Int. J. Electrochem. Sci.*, 2023, **18**(9), 100210, DOI: 10.1016/j.ijoes.2023.100210.

2 D. Sharma, A. Thakur, M. K. Sharma, R. Sharma, S. Kumar, A. Sihmar, H. Dahiya, G. Jhaa, A. Kumar, A. K. Sharma and H. Om, Effective corrosion inhibition of mild steel using novel 1,3,4-oxadiazole-pyridine hybrids: synthesis, electrochemical, morphological, and computational insights, *Environ. Res.*, 2023, **234**, 116555, DOI: 10.1016/j.envres.2023.116555.

3 J. Narenkumar, P. Parthipan and J. Madhavan, Bioengineered silver nanoparticles as potent anti-corrosive inhibitor for mild steel in cooling towers, *Environ. Sci. Pollut. Res.*, 2018, **25**, 5412–5420, DOI: 10.1007/s11356-017-0768-6.

4 D. Sharma, A. Thakur, M. K. Sharma, A. Kumar, K. Jakhar, S. Kumar, A. Sihmar, H. Dahiya, A. Kumar, A. K. Sharma and H. Om, A convenient synthesis, electrochemical profiling, and morphological studies of a pyridine-based 1,3,4-oxadiazole hybrid: a promising study for corrosion mitigation of mild steel in strongly acidic environment, *Inorg. Chem. Commun.*, 2023, **158**(1), 111554, DOI: 10.1016/j.inoche.2023.111554.

5 P. S. Preethi, M. Suganya and J. Narenkumar, *Macrolepiota*-mediated synthesized silver nanoparticles as a green corrosive inhibitor for mild steel in re-circulating cooling water system, *Bioprocess Biosyst. Eng.*, 2022, **45**, 493–501, DOI: 10.1007/s00449-021-02673-w.

6 D. Sharma, A. Thakur, M. K. Sharma, A. Bhardwaj, A. Sihmar, H. Dahiya, A. K. Sharma, A. Kumar, A. Berisha and H. Om, Experimental and computational studies on the corrosion inhibition potential of a novel synthesized thiophene and pyridine-based 1,3,4-oxadiazole hybrid against mild steel corrosion in 1 N HCl, *Environ. Sci. Pollut. Res. Int.*, 2024, DOI: 10.1007/s11356-024-32678-3.

7 G. K. Shamnamol, S. John and J. M. Jacob, Exploring the Corrosion Inhibition Efficacy of Epoxy Merged Silver Nanoparticle Synthesized Using *Garcinia gummi-gutta* Leaf Extract Against Mild Steel in an Acidic Medium, *J. Bio. Tribo Corros.*, 2023, **9**, 81, DOI: 10.1007/s40735-023-00802-4.

8 Z. Zhou, X. Min, S. Wan, J. Liu, B. Liao and X. Guo, A novel green corrosion inhibitor extracted from waste feverfew root for carbon steel in H$_2$SO$_4$ solution, *Results Eng.*, 2023, **17**, 100971, DOI: 10.1016/j.rineng.2023.100971.

9 M. Barbouchi, B. Benzidia, A. Aouidate, A. Ghaleb, M. El Idrissi and M. Choukrad, Theoretical modeling and experimental studies of Terebinth extracts as green corrosion inhibitor for iron in 3% NaCl medium, *J. King Saud Univ., Sci.*, 2020, **32**(7), 2995–3004, DOI: 10.1016/j.jksus.2020.08.004.

10 M. A. Hossein Jafari, A. Dehghani and B. Ramezanzadeh, Investigating the effectiveness of watermelon extract-zinc ions for steel alloy corrosion mitigation in sodium chloride solution, *J. Mol. Liq.*, 2022, **346**, 117086, DOI: 10.1016/j.molliq.2021.117086.

11 M. Ramezanzadeh, Z. Sanaei, G. Bahlakeh and B. Ramezanzadeh, Highly effective inhibition of mild steel corrosion in 3.5% NaCl solution by green Nettle leaves extract and synergistic effect of eco-friendly cerium nitrate additive: experimental, MD simulation and QM investigations, *J. Mol. Liq.*, 2018, **256**, 67–83, DOI: 10.1016/j.molliq.2018.02.021.

12 V. Vorobyova, M. Skiba and K. Andrey, Tomato pomace extract as a novel corrosion inhibitor for the steel in industrial media: the role of chemical transformation of the extract and proinhibition effect, *J. Mol. Struct.*, 2022, **1264**, 133155, DOI: 10.1016/j.molstruc.2022.133155.

13 D. I. Njoku, C. N. Njoku, H. Lgaz, P. C. Okafor, E. E. Oguzie and Y. Li, Corrosion Protection of Q235 Steel in Acidic-Chloride Media Using Seed Extracts of Piper Guineense, *J. Mol. Liq.*, 2021, **330**, 115619, DOI: 10.1016/j.molliq.2021.115619.

14 L. X. Bach, T.-B. Ngoc Dao, K.-L. Duong-Ngo, T. N. Tran, T. L. Minh, H. N. Trong, C. T. Hoang Ngoc, C. Panaitescu, N. T. Hoai and N. N. Dang, Inhibitive behaviours of unripe banana peel extract for mitigating electrochemical corrosion of carbon steel in aggressively acidic solutions, *J. Taibah Univ. Sci.*, 2023, **17**(1), 2247633, DOI: 10.1080/16583655.2023.2247633.

15 L. Huang, W. Q. Chen, S. S. Wang, et al., Starch, cellulose and plant extracts as green inhibitors of metal corrosion: a review, *Environ. Chem. Lett.*, 2022, **20**, 3235–3264, DOI: 10.1007/s10311-022-01400-5.

16 N. Gunavathy and S. C. Murugavel, Corrosion inhibition study of bract extract of Musa acuminata inflorescence on mild steel in hydrochloric acid medium, *IOSR J. Appl. Chem.*, 2013, **5**(2), 29–35.

17 A. Thakur, A. Kumar, S. Kaya, F. Benhiba, S. Sharma, R. Ganjoo and H. Assad, Electrochemical and computational investigations of the *Thysanolaena latifolia* leaves extract: an eco-benign solution for the corrosion mitigation of mild steel, *Results Chem.*, 2023, **6**, 101147, DOI: 10.1016/j.rechem.2023.101147.

18 A. Thakur, O. Dagdag, A. Berisha, E. E. Ebenso, A. Kumar, S. Sharma, R. Ganjoo and H. Assad, Mechanistic insights into the corrosion inhibition of mild steel by eco-benign *Asphodelus tenuifolius* aerial extract in acidic environment: electrochemical and computational analysis, *Surf. Coat. Technol.*, 2024, **480**, 130568, DOI: 10.1016/j.surfcoat.2024.130568.

19 R. T. Loto and O. Olowoyo, Corrosion inhibition properties of the combined admixture of essential oil extracts on mild steel in the presence of SO$_4$$^{2-}$ anions, *S. Afr. J. Chem. Eng.*, 2018, **26**, 35.

20 S. Abrishami, R. Naderi and B. Ramezanzadeh, Fabrication and characterization of zinc acetylacetonate/*Urtica dioica* leaves extract complex as an effective organic/inorganic hybrid corrosion inhibitive pigment for mild steel protection in chloride solution, *Appl. Surf. Sci.*, 2018, **457**, 487.

21 G. Bahlakeh, M. Ramezanzadeh and B. Ramezanzadeh, Experimental and theoretical studies of the synergistic inhibition effects between the plant leaves extract (PLE) and zinc salt (ZS) in corrosion control of carbon steel in chloride solution, *J. Mol. Liq.*, 2017, **248**, 854.

22 U. M. Eduok, S. A. Umoren and A. P. Udoh, Synergistic inhibition effects between leaves and stem extracts of *Sida acuta* and iodide ion for mild steel corrosion in 1 M H_2SO_4 solutions, *Arabian J. Chem.*, 2017, **5**, 325.

23 M. Ali Asaad, N. N. Sarbini, A. Sulaiman, M. Ismail, G. Fahim Huseien, Z. A. Majid and P. B. Raja, Improved corrosion resistance of mild steel against acid activation: impact of novel *Elaeis guineensis* and silver nanoparticles, *J. Ind. Eng. Chem.*, 2018, **63**, 139–148, DOI: 10.1016/j.jiec.2018.02.010.

24 V. S. Aigbodion, Explicit microstructure and electrical conductivity of epoxy/carbon nanotube and green silver nanoparticle enhanced hybrid dielectric composites, *Nanocomposites*, 2022, **7**(1), 35–43, DOI: 10.1080/20550324.2020.1868690.

25 V. S. Aigbodion, Microstructural evolution, electrical conductivity, and electrochemical analysis of α-Al-CNTs-GAg NPs high-conductor nanocomposite, *Chem. Data Collect.*, 2021, **33**, 100707, DOI: 10.1016/j.cdc.2021.100707.

26 C. U. Nwoji, V. S. Aigbodion and J. A. John, Microstructure, electrical conductivity, and wear behavior of aluminum-carbon nanotubes and biosynthesized silver nanoparticles composites, *Int. J. Adv. Manuf. Technol.*, 2021, **115**, 989–1004, DOI: 10.1007/s00170-021-07151-x.

27 E. Ituen and A. Singh, Lin Yuanhua· Onyewuchi Akaranta Green synthesis and anticorrosion effect of *Allium cepa* peels extract-silver nanoparticles composite in simulated oilfield pickling solution, *SN Appl. Sci.*, 2021, **3**, 679, DOI: 10.1007/s42452-021-04670-w.

28 L. X. Bach, T.-B. Ngoc Dao, K.-L. Duong-Ngo, T. N. Tran, T. L. Minh, H. N. Trong, C. T. Hoang Ngoc, C. Panaitescu, N. T. Hoai and N. N. Dang, Inhibitive behaviours of unripe banana peel extract for mitigating electrochemical corrosion of carbon steel in aggressively acidic solutions, *J. Taibah Univ. Sci.*, 2023, **17**(1), 2247633, DOI: 10.1080/16583655.2023.2247633.

29 N. A. Barghout, A. El Nemr and B. A. Abd-El-Nabey, Use of orange peel extract as an inhibitor of stainless steel corrosion during acid washing in a multistage flash desalination plant, *J. Appl. Electrochem.*, 2023, **53**, 379–399, DOI: 10.1007/s10800-022-01772-0.

30 S. I. Ezugha and C. C. Aralu, Evaluation of adsorption and corrosion inhibition properties of *Solanum Macrocarpon* leaves extract on mild steel in sulphuric acid solutions, *SN Appl. Sci.*, 2023, **5**, 381, DOI: 10.1007/s42452-023-05594-3.

31 N. A. Odewunmi, S. A. Umoren and Z. M. Gasem, Utilization of watermelon rind extract as a green corrosion inhibitor for mild steel in acidic media, *J. Ind. Eng. Chem.*, 2015, **21**, 239–247, DOI: 10.1016/j.jiec.2014.02.030.

32 V. Vorobyova, M. Skiba and K. Andrey, Tomato pomace extract as a novel corrosion inhibitor for the steel in industrial media: the role of chemical transformation of the extract and proinhibition effect, *J. Mol. Struct.*, 2022, **1264**, 133155, DOI: 10.1016/j.molstruc.2022.133155.